Dalton Transactions

Accepted Manuscript

ROYAL SOCIETY OF CHEMISTRY

www.rsc.org/dalton

For Table of Contents Only

Anion Coordination Selective [Mn_3] and [Mn_4] Assemblies: Synthesis, Structural Diversity, Magnetic Properties and Catechol Oxidase Activity

Synopsis

The above-mentioned manuscript reports the detail synthesis, characterization, magnetic property and catechol oxidation study of a family of mixed valent ($Mn^{II}Mn^{III}$) and trivalent (Mn^{III}) manganese complexes from a Schiff base ligand. The magnetic behavior of these complexes is dominated by antiferromagnetic exchange coupling. Catechol oxidation study in MeCN revealed that both the trinuclear and tetranuclear complexes are efficient catalysts for the oxidation of 3,5-di-tert-butylcatechol to corresponding quinone by O_2.

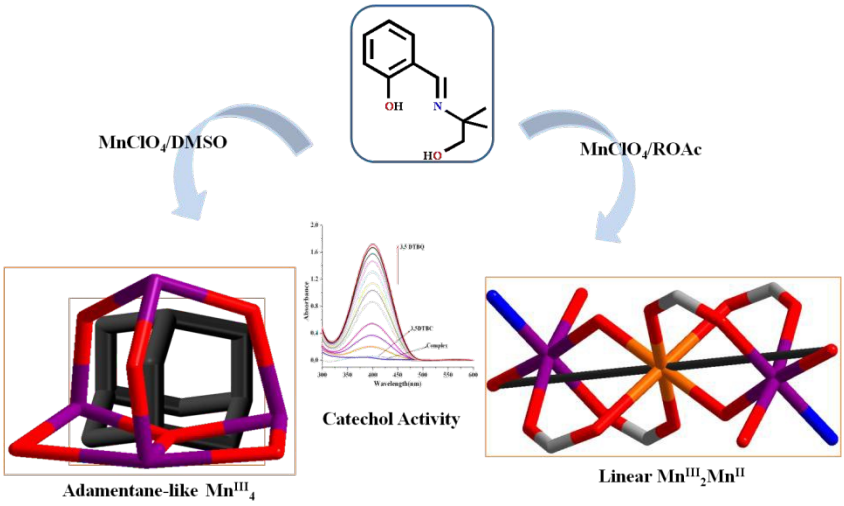

Anion Coordination Selective [Mn_3] and [Mn_4] Assemblies: Synthesis, Structural Diversity, Magnetic Properties and Catechol Oxidase Activity

Moumita Pait,[a] Michael Shatruk[b] and Debashis Ray[a,†]

[a]*Department of Chemistry, Indian Institute of Technology, Kharagpur 721 302, India*

Fax: (+91) 3222-82252; Tel: (+91) 3222-283324; E-mail: dray@chem.iitkgp.ernet.in

[b]*Department of Chemistry & Biochemistry, Florida State University, Tallahassee, FL 32306.*

Abstract

Syntheses, crystal structures, magnetic properties and catechol oxidation behavior are presented for a [Mn_3] and [Mn_4] aggregates, $[Mn^{III}_2Mn^{II}(O_2CMe)_4(dmp)_2(H_2O)_2]\cdot 2H_2O$ (**1**·$2H_2O$), $[Mn^{III}_2Mn^{II}(O_2CCH_2Cl)_4(dmp)_2(H_2O)_2]\cdot H_2O\cdot MeOH$ (**2**·H_2O·MeOH), $[Mn^{III}_4(\mu_3\text{-}O)(dmp)_4(\mu\text{-}DMSO)(N_3)(DMSO)(H_2O)]ClO_4\cdot DMSO$ (**3**·ClO_4·DMSO), and $[Mn^{III}_4(\mu_3\text{-}O)(dmp)_4(\mu\text{-}DMSO)(ClO_4)(DMSO)(H_2O)]ClO_4\cdot DMSO$ (**4**·ClO_4·DMSO), developed with single type ligand H_2dmp, 2-[(2-hydroxy-1,1-dimethyl-ethylimino)-methyl]-phenol. Successful isolation of **1-4** resulted from a systematic exploration of the effect of Mn^{II} salts, added carboxylates, Mn/H_2dmp ratio, presence of azide, and other reaction conditions. The cores of **1** and **2** are similar and consist of a linear $Mn^{III}Mn^{II}Mn^{III}$ unit, in carboxylate and H_2dmp environment, revealing a central Mn^{II} ion in a different environment and terminal Mn^{III} ions available for the introduction of structural and magnetic anisotropy to the system. The cores of **3** and **4** are also similar and consist of a distorted incomplete-adamantane type Mn_4 coordination assembly in carboxylate-free environment built on a triangular [$Mn^{III}_3(\mu_3\text{-}O)$] unit. The magnetic behavior of complexes **1-3** is dominated by antiferromagnetic exchange coupling that results in ground state spin values of $S = 3/2$ for **1** and **2** and $S = 0$ for **3**. In solution all four complexes **1-4** show catechol oxidation activity towards 3,5-DTBC. The catalytic activity for the oxidation of 3,5-DTBC in air followed the order **4** < **3** < **1** < **2**.

Introduction

Multinuclear manganese complexes exhibit a variety of aesthetically pleasing structures that span a range of oxidation states (Mn^{II}, Mn^{III}, and Mn^{IV}).[1-3] These molecular edifices continue to attract synthetic coordination chemists due to their functioning as enzymes mimics, magnetically coupled clusters, and oxidation catalysis.[4, 5] Four manganese centers have been identified in the oxygen-evolving center (OEC) in Photosystem II of plants and cyanobacteria.[6-8] Synthetically controlled aggregation of manganese ions can be tuned to obtain ferromagnetically coupled clusters with large spin ground states.[9-11] Introduction of Mn^{III} ions in such clusters provides the source of significant magnetic anisotropy and can be employed for the design and preparation of single-molecule magnets.[12] Multinuclear complexes containing several Mn centers in close proximity are being utilized for some time as new generation of large-spin molecules with a promise to show SMM behavior, catalytic activity and catechol oxidation.[13] Catechol oxidase is a copper containing type 3 active-site protein that catalyzes the oxidation of a range of o-diphenols (catechols) to o-quinones. Although the catechol oxidases have copper at the active site, investigations have also been shown that some of the Mn(II/III/IV), Ni(II) and Co(II/III) complexes can also promote such activity.[14]

Thus, there continues the need to develop and standardize newer methodologies and synthetic strategies for controlled assembly of multinuclear manganese complexes having interesting magnetic, physical and catalytic properties. Recently [Mn_{12}] clusters have been scrutinized as efficient oxidation catalyst.[15] In recent time, the role of primary ligand system, nature and number of co-ligands and presence of coordinating solvents in the assembly processes has been the topic of contemporary interest. Alcohol-arm bearing tridentate ligands coordinated to a metal ion have the propensity to bind to adjacent metal ions through bridges from their alkoxido groups in deprotonated form. Among the supporting co-ligands, carboxylate and hydroxide groups are versatile in extending bridge structure at the vacant coordination sites around the metal ion. In trying to isolate and study new forms of such coordination clusters, we have been exploring the manganese carboxylate and hydroxide aggregates through the use of a ONO-donor tridentate chelate 2-[(2-hydroxy-1,1-dimethyl-ethylimino)-methyl]-phenol (H_2dmp) (Chart 1). This ligand was used earlier to provide [Ni_3] and [Cu_4] complexes as reported by Dey *et al.*[16] Herein, we present two types of [Mn_3] and [Mn_4] complexes assembled by coordination of ligand-bound mononuclear Mn building units via small ancillary groups.

Chart 1. Ligand used in this work and its binding mode in present [Mn_3] and [Mn_4] complexes.

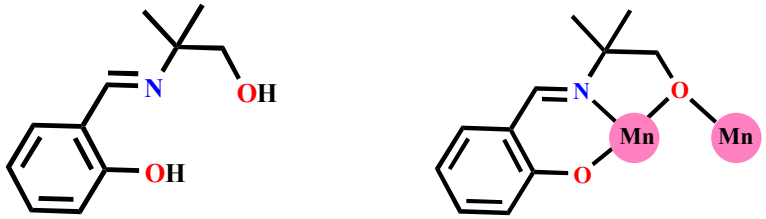

Several reaction systems have been explored, involving carboxylate, azide and carbonate ions and crystallization solvent, DMSO. Carboxylate groups and water molecules function as auxillary bridging and terminal monodenate ligands, respectively, in mixed-valent [Mn_3] complexes, $[Mn^{III}_2Mn^{II}(O_2CR)_4(dmp)_2(H_2O)_2]$ (R =Me, **1** and CH_2Cl, **2**). In the other two complexes, the μ_3-oxido participate in the formation of [$Mn_3(\mu$-O)] unit and support from the DMSO ligand resulted adamantane-like [Mn_4] complexes, $[Mn^{III}_4(\mu_3\text{-}O)(dmp)_4(\mu\text{-}DMSO)(X)(DMSO)(H_2O)]ClO_4$ (X = N_3^-, **3** and ClO_4^-, **4**) in mixed coordination environment. All four complexes have been isolated and crystallographically characterized. Their solid state magnetic properties and solution phase catalytic activity have also been examined.

Experimental Section

Materials. The solvents and chemicals used were obtained from SRL, India, Sigma-Aldrich and Loba Chemie Laboratory Reagents & Fine Chemicals, India. $Mn(ClO_4)_2\cdot 6H_2O$ was freshly prepared by treating manganese carbonate (11.4 g, 0.1 mol) with 12.03 mL of perchloric acid (1:2) and crystallized after concentration on a water bath. Sodium chloroacetate was prepared by treating chloroacetic acid (14.1 g, 0.15 mol) with solid sodium hydroxide (6.0 g, 0.15 mol) followed by concentration and crystallization on a water bath. All other chemicals and solvents were reagent grade and used as received without further purification.

Caution!! *Although no such behavior was observed during the present work, azide and perchlorate salts involving organic ligands are potentially explosive; such compounds should be synthesized and used in small quantities, and treated with utmost care at all times.*

Syntheses. H_2**dmp Ligand**. 2-[(2-Hydroxy-1,1-dimethyl-ethylimino)-methyl]-phenol used in the present work was prepared from a single-step condensation of salicylaldehyde (1.0 mL, 10 mmol) with 2-amino-2-methyl-1-propanol (0.952 g, 10 mmol) in MeOH (25 mL) under reflux

for 1 h. The product was obtained as a yellow solid by triturating with hexane and was further recrystallized from MeOH as reported earlier.[16]

$[Mn^{III}_2Mn^{II}(O_2CMe)_4(dmp)_2(H_2O)_2]\cdot 2H_2O$ (**1**·$2H_2O$). To a stirred yellow MeOH solution (10 mL) of H_2dmp (0.19 g, 1.0 mmol), a MeOH solution (10 mL) of $Mn(ClO_4)_2\cdot 6H_2O$ (0.54 g, 1.5 mmol) was added slowly followed by dropwise addition of NEt_3 (0.27 mL, 2.0 mmol) with stirring at room temperature in air. The orange solution formed initially changed to brown after complete addition of NEt_3. The resulting brown solution was stirred for *ca.* 15 min, and a solution of NaOAc (2 mL, 0.16g, 2.0 mmol) was added dropwise to the mixture. The solution immediately turned reddish brown and was stirred for another 2 h. The brown solution formed was then filtered and the filtrate was layered with equal volume of CH_2Cl_2. Brown single crystals of **1**·$2H_2O$ suitable for X-ray diffraction were obtained after 7 days. Yield of the crystalline compound based on total Mn was 0.294 g (66%). Anal. Calc. for $C_{30}H_{50}Mn_3N_2O_{18}$ (891.54 g mol^{-1}): C, 40.42; H, 5.65; Mn, N, 3.14. Found: C, 40.05; H, 5.89; N, 3.08. Molar conductance, Λ_M (MeOH solution): 28.5 S m^2 mol^{-1}. Selected FT-IR bands: (KBr, cm^{-1}) 3369 (br), 1588 (vs) and 1411 (vs). UV-vis spectra [λ_{max}, nm (ε, M^{-1} cm^{-1})]: (MeCN solution) 382 (5150), 233 (42625).

Alternative method of preparation of 1. To a yellow MeOH solution (10 mL) of H_2dmp (0.19 g, 1.0 mmol), a MeOH solution (10 mL) of $Mn(OAc)_2\cdot 4H_2O$ (0.18 g, 1.5 mmol) was added slowly followed by dropwise addition of NEt_3 (0.27 mL, 2.0 mmol) with stirring at room temperature in air. The stirring of the red-brown solution was continued for 2 h. The brown solution formed was then filtered and the filtrate was layered with CH_2Cl_2. Brown single crystals suitable for X-ray diffraction were obtained after 5 days.

$[Mn^{III}_2Mn^{II}(O_2CCH_2Cl)_4(dmp)_2(H_2O)_2]\cdot H_2O\cdot$MeOH. (**2**·$H_2O$·MeOH). Compound **2** was obtained following a method similar to that described above for **1** by using NaO_2CH_2Cl (0.46 g, 2.0 mmol) in place of NaOAc. After about one week brown needle shaped crystals suitable for X-ray study were obtained. Yield of the crystalline compound based on total Mn was 0.308 g, 59%. Anal. Calc. for $C_{32}H_{48}Cl_4Mn_3N_2O_{18}$ (1055.34 g mol^{-1}): C, 36.42; H, 4.58; N, 2.65; Found: C, 36.28; H, 4.45; N, 2.51. Molar conductance, Λ_M (MeOH solution): 35 S m^2 mol^{-1}. Selected FT-IR bands (KBr, cm^{-1}): 3427 (br), 1618 (s), 1570 (m) and 1385 (m). UV-vis spectra [λ_{max}, nm (ε, M^{-1} cm^{-1})] (MeCN solution): 385 (8480), 236 (48910).

Alternative method of preparation of 2. The same procedure was employed as described for **1**, except for the use of $Mn(O_2CCH_2Cl)_2.4H_2O$ (0.46 g, 1.5 mmol) in place of $Mn(OAc)_2 \cdot 4H_2O$. Dark-brown crystals were obtained after 6 days.

$[Mn^{III}_4(\mu_3\text{-}O)(dmp)_4(\mu\text{-}DMSO)(N_3)(DMSO)(H_2O)]ClO_4 \cdot DMSO$ (3·ClO_4·DMSO**).** To a stirred yellow MeOH solution (10 mL) of H_2dmp (0.19 g, 1.0 mmol), a MeOH solution (10 mL) of $Mn(ClO_4)_2 \cdot 6H_2O$ (0.36 g, 1 mmol) was added slowly followed by dropwise addition of NEt_3 (0.27 mL, 2.0 mmol) with stirring at room temperature in air. The orange solution formed initially changed to brown after complete addition of NEt_3. The resulting brown solution was stirred for *ca.* 15 min, and then an aqueous solution of NaN_3 (2 mL, 0.065 g, 1.0 mmol) was added dropwise to the mixture resulting in the formation of a dark brown solution after 1 h. The reaction mixture was evaporated in air to give a brown powder, which was isolated by filtration, washed with cold MeOH and dried under vacuum over P_4O_{10}. X-ray quality deep-brown crystals of **3** were obtained by vapor diffusion of Et_2O into a DMSO solution (v/v 1:1) of complex over 2 months. Yield: 0.085 g, 24% (based on Mn). Anal. Calc. for $C_{50}H_{70}ClMn_4N_7O_{17}S_3$ (1392.52 g mol^{-1}): C, 43.13; H, 5.07; N, 7.04; Found: C, 43.19; H, 5.25; N, 7.03. Molar conductance, Λ_M (MeOH solution): 102 S m^2 mol^{-1}. Selected FT-IR bands (KBr, cm^{-1}): 3409 (br), 2027 (s), 1616 (s), 1303 (s), 1093 (s), 1047 (m), 762 (m) and 664 (m). UV-vis spectra [λ_{max}, nm (ε, $M^{-1}cm^{-1}$)] (MeCN solution): 390 (9622), 575 (1755), 256 (13295).

$[Mn^{III}_4(\mu_3\text{-}O)(dmp)_4(\mu\text{-}DMSO)(ClO_4)(DMSO)(H_2O)]ClO_4 \cdot DMSO$ (**4**·ClO_4·DMSO). Solid Na_2CO_3 (0.21 g, 2.0 mmol) was added to a stirred MeOH solution (10 mL) of the ligand (0.19 g, 1.0 mmol) and stirring was continued for 2 h. To this yellow solution a MeOH solution (10 mL) of $Mn(ClO_4)_2 \cdot 6H_2O$ (0.36 g, 1.0 mmol) was added and the mixture was stirred for 1 h to afford a dark brown solution. The solution was evaporated in air to give a brown powder, which was isolated by filtration, washed with cold MeOH and dried under vacuum over P_4O_{10}. The powder was dissolved in DMSO and layered with Et_2O (v/v 1:1). Dark-brown crystals suitable for X-ray diffraction were obtained after 15 days. The yield of the crystalline material based on total Mn was 18% (0.067 g). Anal. Calcd for $C_{50}H_{70}Cl_2Mn_4N_4O_{21}S_3$ (1449.94 g mol^{-1}): C, 41.42; H, 4.87; N, 3.86; Found: C, 41.29; H, 4.95; N, 3.39. Molar conductance, Λ_M (MeOH solution): 113 S m^2 mol^{-1}. Selected FTIR bands (KBr, cm^{-1}): 3368 (br), 1670 (s), 1203(s), 1130 (s) and 1046 (m).

UV-vis spectra [λ_{max}, nm (ε, L mol^{-1} cm^{-1})] (MeCN solution): 389 (10608), 575 (1755), 260 nm (13970).

Physical Measurements. Elemental analyses (CHN) were performed with a Perkin-Elmer model 240C elemental analyzer. FT-IR spectra were recorded on a Perkin-Elmer 883 spectrometer. The solution electrical conductivity and electronic absorption spectra were obtained using a Unitech type U131C digital conductivity meter with a solute concentration of about 10^{-3} *M* and a Shimadzu UV 3100 UV-vis-NIR spectrophotometer respectively.
Magnetic measurements were performed on microcrystalline samples of **1-4** using a Quantum Design SQUID magnetometer MPMS-XL. DC magnetic susceptibility was measured in an applied field of 0.1 T, in the 1.8–300 K temperature range. Isothermal dependences of magnetization were measured at 1.8 K with the magnetic field varying from 0 to 7 T. The data were corrected for the diamagnetic contribution from the sample holder and for the intrinsic diamagnetism of the sample using tabulated constants.[17]

X-ray Crystallography. Suitable single crystals of **1**·H_2O, **2**·H_2O·MeOH, **3**·ClO_4·DMSO and **4**·ClO_4·DMSO were examined using a Bruker SMART APEX-II CCD diffractometer, equipped with a fine focus 1.75 kW sealed tube Mo-K_α radiation (λ) 0.71073 (Å). The data were collected at 298 K, by scanning over the ω angle at a step of 0.3° and a scan speed of 5 s per frame. The SMART software was used for data acquisition. Data integration and reduction were performed with SAINT and XPREP software.[18] Multiscan empirical absorption corrections were applied to the data using the program SADABS.[19] Structures were solved by direct methods using SHELXS-97[20a] and refined with full-matrix least squares on F^2 using SHELXL-97.[20b] The locations of the heaviest atoms (Mn) were easily determined, and the O, N, and C atoms were subsequently determined from the difference Fourier maps. The non-H atoms were refined anisotropically (except the S6 and O33b of DMSO molecule). The H atoms were introduced in calculated positions and refined with fixed geometry and riding thermal parameters with respect to their carrier atoms. The high R_1/wR_2 = 0.0828/0.2539 for complex **4** is due to the presence of disordered DMSO molecules and quality of data set used for structure solution. Despite several attempts we were not able to obtain better quality crystals for the compound. A summary of the crystal data and relevant refinement parameters are given in Table 1. CCDC 1007135 (**1**), 1007136 (**2**), 1007137 (**3**) and 1007138 (**4**) contain the supplementary crystallographic data for

this paper. These data can be obtained free of charge at www.ccdc.cam.ac.uk/conts/retrieving.html (or from the Cambridge Crystallographic Data Centre, 12, Union Road, Cambridge CB2 1EZ, U.K.; fax, +44-1223/336-033; e-mail, deposit@ccdc.cam.ac.uk). CCDC No. 1007135-1007138.

Table 1. Crystal structure parameters and refinement data for **1**·H_2O, **2**·H_2O·MeOH, **3**·ClO_4·DMSO and **4**·ClO_4·DMSO.

Parameters	**Complex 1**	**Complex 2**	**Complex 3**	**Complex 4**
Formula	$C_{30}H_{50}Mn_3N_2O_{18}$	$C_{32}H_{48}Cl_4Mn_3N_2O_{18}$	$C_{50}H_{70}ClMn_4N_7O_{17}S_3$	$C_{50}H_{70}Cl_2Mn_4N_4O_{21}S_3$
F.W.	891.54	1055.34	1392.52	1449.94
Crystal system	Triclinic	Monoclinic	Monoclinic	Monoclinic
Space group	*P*-1	*P* $2_1/c$	*P* $2_1/c$	*P* $2_1/c$
Crystal color	Brown	Brown	Brown	Brown
Crystal size/mm^3	0.32x0.26x0.21	0.31x0.25x0.20	0.35x0.29x0.26	0.34x0.26x0.23
a/Å	9.875(2)	11.357(6)	11.9220(9)	11.6789(18)
b/Å	10.924(2)	10.602(5)	12.4025(9)	45.485(7)
c/Å	11.134(2)	18.852(9)	42.763(3)	16.2162(19)
α/°	95.459(6)	90.00	90.00	90.00
β/°	114.801(5)	106.516(16)	96.768(2)	131.030(7)
γ/°	111.466(5)	90.00	90.00	90.00
V/$Å^3$	969.7(3)	2176.3(19)	6279.0(8)	6498.3(16)
Z	1	2	4	4
D_c/g cm^{-3}	1.527	1.610	1.473	1.482
μ (mm^{-1})	1.037	1.176	0.998	1.010
F(000)	463	1082	2880	2992
T/K	298(2)	298(2)	298(2)	298(2)
Total reflns	13150	23774	79807	62705
R(int)	0.0347	0.1447	0.1150	0.0927
Unique reflns	4739	4983	12849	11634
Observed reflns	3236	3280	6961	7070
Parameters	269	289	739	761
R_1; wR_2 ($I > 2\sigma(I)$)	0.0395, 0.1032	0.0788, 0.2346	0.0755, 0.2351	0.0828, 0.2539
GOF (F^2)	1.047	1.034	1.045	1.038
Largest diff peak and hole (e $Å^{-3}$)	0.424, -0.499	1.687, -1.242	1.622, -0.923	2.029, --1.192

$R_1 = \Sigma(||F_o|-|F_c||)/\Sigma|F_o|$. $wR_2 = [\Sigma w(|F_o|-|F_c|)^2/\Sigma w(F_o)^2]^{1/2}$. $w = 0.75/(\sigma^2(F_o) + 0.0010F_o^2)$

Results and Discussion

Syntheses. Two methods have been employed in this work to prepare [Mn_3] and [Mn_4] aggregates using a common alcohol-arm bearing ligand H_2dmp (Scheme S1, ESI). The first one uses the reaction with $Mn(ClO_4)_2$ in the presence of added carboxylates and the second one employs $Mn(ClO_4)_2$ in the absence of any carboxylate but with sodium azide and sodium carbonate. In all reactions atmospheric oxygen was used for the partial or complete oxidation of Mn^{II} to Mn^{III}. Various synthetic conditions and reaction systems had been explored with other added ancillary groups before the following reproducible synthetic procedures were established. Tridentate ONO donor ligands are known to support the growth of multinuclear assemblies.[21] The reaction of $Mn(ClO_4)_2$ with H_2dmp and $MeCO_2Na$ in a 3:2:4 molar ratio in MeOH, with or without added NEt_3, led to the formation of compound **1**. The use of NEt_3 followed by crystallization from MeOH-CH_2Cl_2 provided **1** in ~66% yield. On the other hand, the reaction without NEt_3 demanded longer stirring time (>6 h) to get the red-brown solution, and the yield was considerably lower (~20%). The same reaction using $ClCH_2CO_2Na$ in place of $MeCO_2Na$ led to compound **2** in 59% yield. The chemical reactions for the generation of **1** and **2** are summarized in Eqs. 1 and 2 below.

$$3Mn(ClO_4)_2\cdot 6H_2O + 2\ H_2dmp + 4NaOAc + 2NEt_3 + O_2 \xrightarrow{MeOH}$$
$$[Mn_3(dmp)_2(O_2CMe)_4(H_2O)_2]\cdot 2H_2O + 2(NHEt_3)(ClO_4) + 4NaClO_4 + 16H_2O \quad ...(1)$$

$$3Mn(ClO_4)_2\cdot 6H_2O + 2\ H_2dmp + 4NaO_2CH_2Cl + 2NEt_3 + O_2 \xrightarrow{MeOH}$$
$$[Mn_3(dmp)_2(O_2CCH_2Cl)_4(H_2O)_2]\cdot H_2O\cdot MeOH + 2(NHEt_3)(ClO_4) + 4NaClO_4 + 16H_2O \quad ...(2)$$

During the formation of **1** and **2** in solution, most likely the single phenoxido coordination initially forms the mononuclear trivalent species [Mn^{III}(dmp)(carboxylate)$(H_2O)_2$]. Simultaneously, if [Mn^{II}(carboxylate)$_2$] species is also formed in solution, two of [Mn^{III}(dmp)(carboxylate)$(H_2O)_2$] can trap it to yield **1** and **2** depending on the carboxylates used (Schemes S2 and S3, ESI). Thus, the structure is composed of two terminal mononuclear units of [Mn^{III}(dmp)(RCOO)(H_2O)] connected by a central [$Mn^{II}(RCOO)_2$] unit through the alkoxido oxygen atoms of the ligand and the oxygen atoms of carboxylate anions. We have tried another

reaction using NaN_3 in place of sodium carboxylates in the previous reactions (1) and (2). The reaction of $Mn(ClO_4)_2$, ligand, NaN_3 and NEt_3 in 2:2:2:1 molar ratio in MeOH in air produced a red-brown powder in 62% yield. Several pure and mixed organic solvents were employed to grow X-ray diffraction quality single crystals of this red-brown product. Only 1:1 DMSO-Et_2O mixture afforded brown single crystals of **3** in 24% yield after two months, and X-ray analysis established it as $[Mn_4(\mu_3\text{-}O)(dmp)_4(\mu\text{-}DMSO)(N_3)(DMSO)(H_2O)]ClO_4\cdot DMSO$. The presence of the single anionic fragment within the tetranuclear aggregate was further confirmed by an analogous reaction using Na_2CO_3 in place of NaN_3. The reaction of $Mn(ClO_4)_2$, H_2dmp, and Na_2CO_3 in 2:2:1 molar ratio in MeOH initially afforded the powder material which on treatment with 1:1 DMSO-Et_2O solvent mixture afforded $[Mn_4(\mu_3\text{-}O)(dmp)_4(\mu\text{-}DMSO)(ClO_4)(DMSO)(H_2O)]\cdot ClO_4\cdot DMSO$ (**4**) in 18% yield. The DMSO-Et_2O (1:1) solvent mixture is a unique one for the slow and smooth recrystallization process. The reactions for the generation of **3** and **4** are summarized in Eqs. 3 and 4, respectively.

$$4Mn(ClO_4)_2\cdot 6H_2O + 4dmpH_2 + 2NaN_3 + 4NEt_3 + 2O_2 \xrightarrow{MeOH} [\text{Brown powdered intermidiate}]$$

$$\xrightarrow{DMSO\text{-}Et_2O} [Mn_4(\mu_3\text{-}O)(dmp)_4(\mu\text{-}DMSO)(N_3)(DMSO)(H_2O)]ClO_4\cdot DMSO + 4(NHEt_3)(ClO_4) + NaClO_4 + 2HClO_4 + 27H_2O \quad ...(3)$$

$$4Mn(ClO_4)_2\cdot 6H_2O + 4dmpH_2 + 2Na_2CO_3 + 2O_2 \xrightarrow{MeOH} [\text{Brown powdered intermidiate}]$$

$$\xrightarrow{DMSO\text{-}Et_2O} [Mn_4(\mu_3\text{-}O)(dmp)_4(\mu\text{-}DMSO)(ClO_4)(DMSO)(H_2O)]ClO_4\cdot DMSO + 4(NHEt_3)(ClO_4) + 2NaClO_4 + 2HClO_4 + 27H_2O \quad \ldots(4)$$

A different kind of aggregation processes took place to provide $[Mn_4]$ coordination clusters **3** and **4** in absence of carboxylates and in presence of azide and perchlorate anions. Initially in solution, the most probable precursor species formed is $[Mn^{III}(dmp)(ClO_4)(H_2O)_2]$. In the following step DMSO as solvent of crystallization coordinate in two different modes to the Mn centers and plays crucial role for $[Mn_4]$ aggregate formation. In these two aggregates, two DMSO groups are present as neutral monodentate and bridging O donor ligands (Schemes S3 and S4, ESI). [21]

The elemental analysis of solid samples and molar conductivity studies in respective solutions also conform the above formula of the four compounds. The nature and composition of the final

complex is thus greatly influenced by the presence of the ancillary ligands and crystallizing solvent pair.

FT-IR Spectra

All the three complexes exhibit characteristic stretching frequencies for the dmp^{2-} ligand anion bound to the manganese centers (Fig. S1 and S2, ESI). The $\bar{\nu}_{C=N}$ stretching vibrations of manganese-bound imine functionalities are observed at 1601-1618 cm^{-1} for **1**-**4**. For **1** and **2**, the asymmetric $\bar{\nu}_{as(COO)}$) stretching vibrations of the four bound carboxylate groups are detected at 1562 and 1570 cm^{-1}, respectively, while the symmetric ($\bar{\nu}_{s(COO)}$) stretching vibrations are observed at 1411 and 1385 cm^{-1}, respectively. The differences in these two types of stretching frequencies ($\Delta\bar{\nu} = \bar{\nu}_{as(COO)} - \bar{\nu}_{s(COO)}$) are 151 and 185 cm^{-1}, respectively, which are characteristic of $\mu_{1,3}$-bridging carboxylates in **1** and **2.**[22] In complex **3**, a strong band at 2027 cm^{-1} is assigned to the asymmetric stretching vibration, ν_{as}(NNN), of the azide group terminally bound to the Mn^{III} center.[23] Characteristic stretching vibrations for the [Mn_3O] base units were observed at 663 and 615 cm^{-1} for **3** and **4**, respectively.[24] In addition to these, very strong bands at ~1095 cm^{-1} for **3** and **4** are attributed to the uncoordinated ClO_4^- anions. For **4,** the stretching frequencies for one coordinated ClO_4^- ion appear at 1203, 1182 and 1130 cm^{-1}, corresponding to the triply degenerate ν_3 mode of vibration of the tetrahedral $C1O_4^-$ ion.[25] Another characteristic set of resonances at 1027 and 762 cm^{-1} in **3** and 1045 and 722 cm^{-1} in **4** was assigned to the ν_{as}(S−O) and ν_{as}(C−S) asymmetric stretching vibrations of DMSO molecules. The ν_{as}(S−O) stretching frequency for free DMSO appears at 1055 cm^{-1}, which is shifted to low energy by 27 and 10 cm^{-1} for **3** and **4**, respectively.[26] This shift in S−O stretching frequencies also confirms the monodentate and bridging coordination of DMSO molecules through their oxygen atoms.[27]

Electronic Spectra

The electronic absorption spectra of [Mn_3] and [Mn_4] complexes have been measured in MeCN. Complexes **3** and **4** exhibit absorption shoulders around 575 nm for the manganese(III)-based d–d transition.[28] The intensities of the other manganese based d–d transition are very low and observed at 382-390 nm with ε values of 4785-10610 $M^{-1}\,cm^{-1}$ for all four complexes. The bands in the range of 400-200 nm are likely to be of charge-transfer origin. In MeCN solutions, the band below 300 nm *viz*., at 233 (ε, 42625 $M^{-1}\,cm^{-1}$), 236 (ε, 48910 $M^{-1}\,cm^{-1}$), 256 (13295 M^{-1}

cm^{-1}) and 260 nm (ε, 13970 M^{-1} cm^{-1}) for **1-4**, respectively, originate from the π ⟶ π* transitions associated with the azomethine group.[29]

Crystal Structures Description

1·2H₂O and 2·H₂O·MeOH. The structures of mixed valence neutral units $[Mn_3(O_2CMe)_4(dmp)_2(H_2O)_2]$ and $[Mn_3(O_2CCH_2Cl)_4(dmp)_2(H_2O)_2]$ in **1** and **2**, respectively, are shown in Fig. 1 and selected bond distances and angles are summarized in Tables 1 and S1(ESI). Complex **1** crystallizes in the triclinic *P*$\bar{1}$ space group while **2** crystallizes in the monoclinic $P2_1/c$ space group. The central manganese ion is located at a crystallographic inversion center. Each dmp^{2-} provides a tridentate ONO donor chelation mode to a terminal Mn^{III} ion (Mn1) where alkoxido O atom bridges to the central Mn^{II} ion (Mn2). Each $Mn^{III}Mn^{II}$ pair is also bridged by two $\eta^1:\eta^1$:μ-acetato linkers which complete the hexa-coordinate environments around three Mn ions. The structural analyses reveal a linear $Mn^{III}Mn^{II}Mn^{III}$ unit with the Mn···Mn···Mn angle 180° (Fig. S3, ESI). The Mn oxidation states were evident from the metric parameters and the Jahn-Teller axial elongation at the two terminal Mn^{III} ions along Mn1−O6 (2.207, 2.242 Å) and Mn1−O7 (2.340, 2.255 Å) bonds, and were confirmed by BVS calculations (Table S2, ESI).[30] The identification of the Jahn-Teller axis on each Mn^{III} center defines the *basal* plane consisting of O1, O2, O4 and N1 atoms with distances range within 1.873-2.004 Å for **1** and **2**.

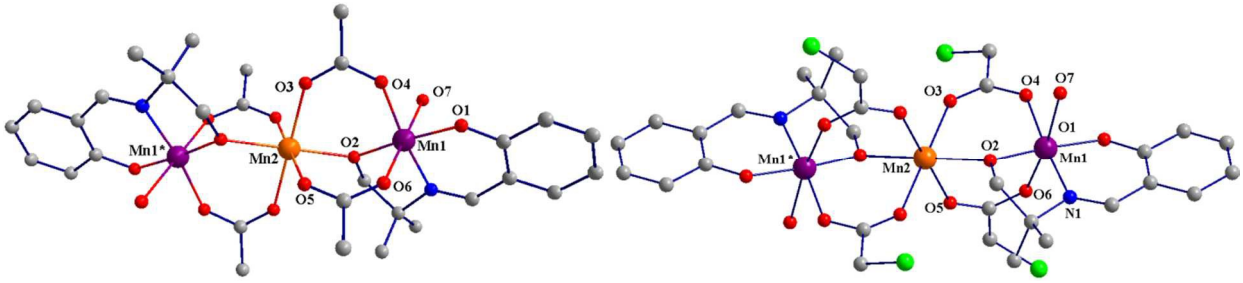

Fig. 1 Structure of the neutral trinuclear units of **1** (left) and **2** (right) with partial atom-numbering scheme. H atoms and lattice solvent molecules have been omitted for clarity. Color code: Mn^{III}, purple; Mn^{II}, orange; O, red; N, blue; C, grey; Cl, green.

For these two complexes the Mn-O_{carb} (carb = carboxylate) distances from manganese in +2 and +3 oxidation states for μ:$\eta^1:\eta^1$-carboxylato bridges fall within 1.956–2.246 Å range. The Mn^{III}-

O_{carb} distances are shorter (1.956-2.207 Å) compared to the Mn^{II}-O_{carb} distances (2.140-2.207 Å). Around the central Mn^{II} atom, the O_6 environment is less distorted (the angles between *cis* atoms are 87.5–92.5° and *trans* atoms is 180°) compared to the terminal NO_5 environments (angles between *cis* and *trans* atoms range in 83.4–98.5° and 170.2–179.5°, respectively) (Fig. 2). In complex **1**, the Mn(1)···Mn(2) and Mn(1)···Mn(1*) distances of 3.476(7) and 6.953(1) Å, respectively, are shorter than those in **2** at 3.520(2) and 7.040 Å, respectively.

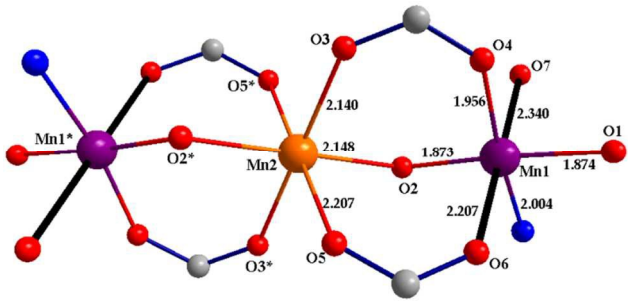

Fig. 2 Core structure of **1** (with unique bond distances in Å), with the O-Mn-O Jahn−Teller axes on the terminal atoms indicated as black bonds. Color code: Mn^{III}, purple; Mn^{II}, orange; O, red; N, blue; C, grey. Atoms labeled with * were generated from the parent atoms by inversion through the Mn2 center.

Analysis of the crystal packing of the trinuclear complexes **1** and **2** reveals the presence of extensive noncovalent interactions. One water molecule in **1** and one water and one MeOH molecules in **2** are present as solvent of crystallization. The packing diagram for **1** along the *a* axis shows well-isolated trinuclear complexes that are organized in layers with the water molecules occupying the space within these layers. The closest intermolecular Mn···Mn distances between adjacent layers are 7.150 and 9.515 Å for **1** and **2**, respectively. The intermolecular separations within the same layer are 6.576 and 5.406 Å for **1** and **2**, respectively (Fig. 3). There are hydrogen bonding interactions involving the bridging acetate ligands and the lattice water molecules. The complexes further show strong π···π (phenyl) interaction between the neighboring Mn_3 units (Fig. 3). The distance between H7 of one phenyl ring and the phenyl ring of next layer is 3.261 Å.

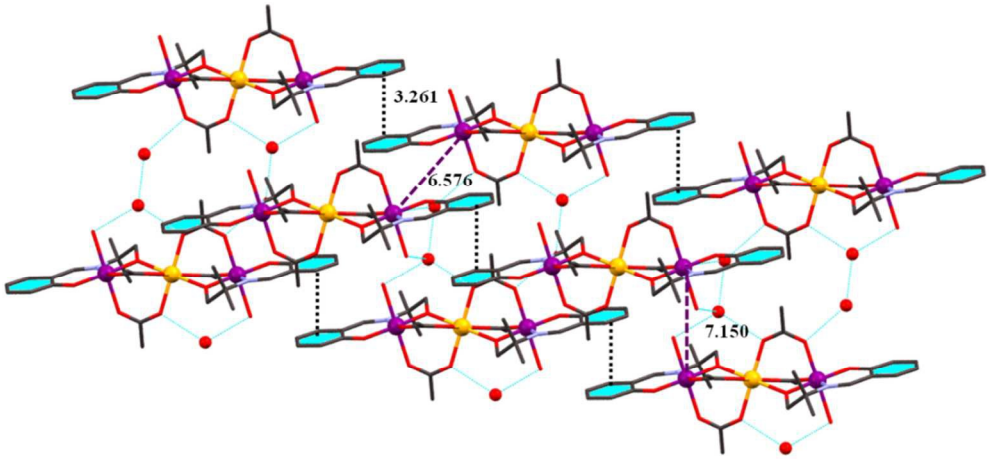

Fig. 3 H-bonding and π-π interaction present in complex **1**

The type of linear $Mn^{III}_2Mn^{II}$ arrangement reported in this work for **1** and **2** is rare in the literature.[31] The $Mn^{II}_2Mn^{III}$ core is known earlier in two examples, one of which is a SMM.[31-33] There are other examples of linear Mn_3 units in other combination of oxidation states which include Mn^{II}_3,[34] $Mn^{II}Mn^{III}Mn^{IV}$,[35] and Mn^{IV}_3.[36]

Table 2. Selected bond distances (Å) of complexes **1**·2H_2O and **2**·H_2O·MeOH

Complex 1·2H_2O			
Mn1-O2	1.873(16)	Mn1-O7	2.340(2)
Mn1-O1	1.873(17)	Mn2-O3	2.140(19)
Mn1-O4	1.956(18)	Mn2-O2	2.148(16)
Mn1-N1	2.004(2)	Mn2-O5	2.206(19)
Mn1-O6	2.2073(19)	Mn1···Mn2	3.477(5)

Complex 2·H_2O·MeOH			
Mn1-O1	1.868(4)	Mn1-O7	2.255(6)
Mn1-O2	1.868(4)	Mn2-O2	2.131(4)
Mn1-O4	1.976(4)	Mn2-O5	2.189(5)
Mn1-N1	1.997(5)	Mn2-O3	2.153(4)
Mn1-O6	2.244(5)	Mn1···Mn2	3.522(1)

3*·*ClO₄*·*DMSO and 4*·*ClO₄*·*DMSO. The tetranuclear structures of cationic fragments $[Mn_4^{III}(\mu_3\text{-}O)(\mu\text{-dmp})_4(\mu\text{-DMSO})(DMSO)(X)(H_2O)]^+$ (X = N_3^- and ClO_4^-) in **3** and **4**, respectively) are

shown in Fig. 4 and selected inter atomic distances and angles are summarized in Table 3 and S3 (ESI). Complexes **3** and **4** crystallize in monoclinic $P2_1/c$ space group and the asymmetric units for the two compounds contain the whole Mn_4 unit, one perchlorate counter anion and one DMSO molecule as solvent of crystallization. Each dmp^{2-} shows tridentate chelation to one of the four Mn^{III} ions present in the cluster with terminal alkoxido group bridging to the adjacent Mn^{III} ions (Fig. 5). The asymmetric cationic units consist of a planar triangular Mn^{III}_3 unit tightly bridged by a central μ_3-O atom derived from a solvent water molecule. For compound **3**, this μ_3-O^{2-} ion lays 0.118 Å below the plane of the three Mn ions. The $[Mn_3O]$ unit accepts the fourth Mn atom through one alkoxido bridge donation and two alkoxido bridge acceptances from the Mn^{III} bound ligand alcohol arms. Two solvent DMSO molecules show bridging and terminal coordination to three Mn ions within the $[Mn_3O]$ entity. Finally, one N_3^-/ClO_4^- ion and one solvent water molecule on two Mn ions complete the six-coordination environment around each Mn ion. The μ_3-oxido supported $[Mn_3]$ unit attaches the fourth Mn atom (Mn4) through acceptance of two ligand alkoxido (O_{alk}) bridges of ligand bound Mn2 and Mn3 centers, and donation of its own ligand alkoxido (O_{alk}) bridge to Mn1.

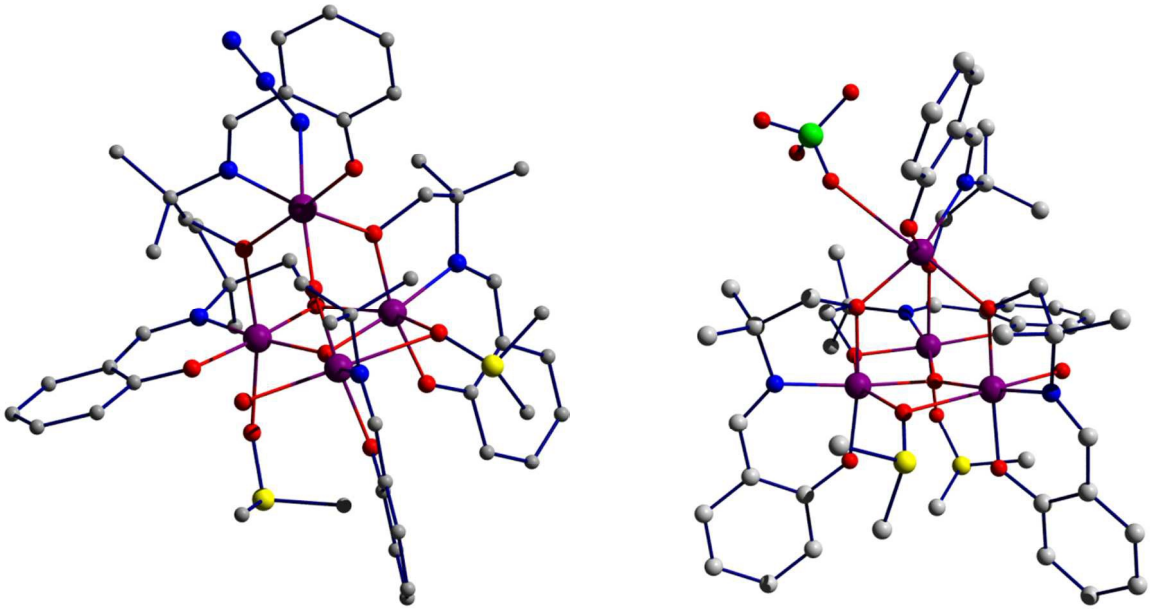

Fig. 4 Structure of the cationic tetranuclear units of **3** (left) and **4** (right). H atoms and lattice solvent molecules have been omitted for clarity. Color code: Mn^{III}, purple; O, red; N, blue; C, grey; S, yellow.

The *cis* and *trans* angles vary within 76.2-101.8 and 155.3–174.9°, respectively, which clearly indicate the distortions within the tetranuclear molecules resulting in strained structures (Table

S2, ESI). Both compounds thus contain a pseudo-adamantane [Mn_4O_{10}] unit supported by oxido, alkoxido and DMSO bridges. The Mn oxidation states were confirmed by BVS calculations (Table S2, ESI). As expected, all four Mn^{III} centers exhibit Jahn-Teller axial elongation along the O7–Mn1–O11, O4–Mn2–O9, O1–Mn3–O2 and N5–Mn4–O8 (O13–Mn4–O8 in case of complex 4) axes with bond distances in the range of 2.174 to 2.732 Å (Fig. S4). The oxido nucleus of the [Mn_3O] unit registers shorter Mn−O distances in 1.894-1.927 Å range and responsible for three Mn···Mn separations of 2.997 to 3.516 Å within this unit. The fourth Mn ion, in this pseudo-adamantane structure, records three other Mn···Mn distances at 3.550, 3.670 and 3.671Å (Fig. 8a). All these distances are close to other reported μ_4-oxido bridged [Mn_4O] units showing Mn···Mn distances in 2.819-3.734 Å range.[37]

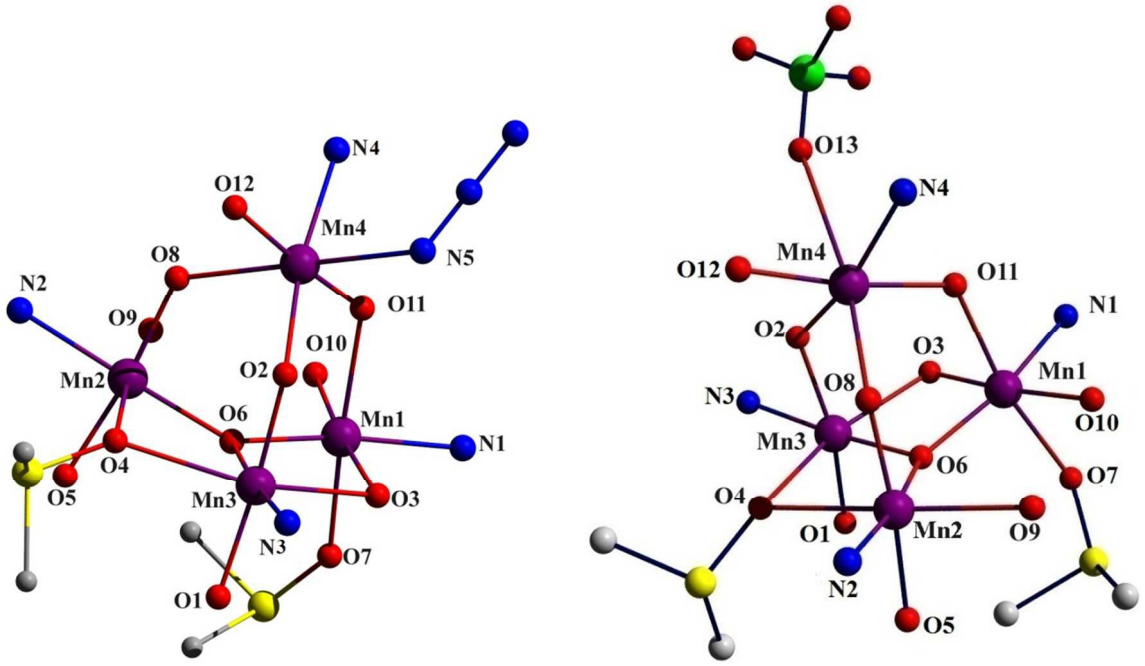

Fig. 5 The atom connectivity in the core of **3**·ClO_4·DMSO (left) and **4**·ClO_4·DMSO with partial atom numbering schemes. Color code: Same as Fig. 4.

The asymmetric nature of the μ_3-oxido bridge is confirmed from the varying magnitudes of Mn−O−Mn angles in 102-136º range. Three Mn^{III} ions in [Mn_3O] unit are in NO_5 environment, whereas the fourth one has N_2O_4 surroundings (Fig. 5). Interestingly, the DMSO molecules showed two types of binding modes which are not routinely seen in other known manganese coordination aggregates, one in a monodentate O donor mode and the other in a $\mu_{1,1}$-O fashion.[38] The monodentate azide N and perchlorate O atoms show weak and distal binding to the fourth

Mn ion at 2.325 and 2.732 Å in **3** and **4**, respectively. The terminally bound water molecules of Mn2 centers were engaged in intramolecular H-bonding interactions with the Mn1 bound phenoxido O atoms in **3** and **4** at 2.697 and 2.704 Å, respectively (Fig. S5, ESI).

Table 3 Selected bond distances (Å) for **3**·ClO_4·DMSO and **4**·ClO_4·DMSO

3·ClO_4·DMSO			
Mn1-O3	1.884(4)	Mn3-O1	1.877(5)
Mn1-O10	1.911(4)	Mn3-O2	1.938(4)
Mn1-O11	2.247(4)	Mn3-O3	2.174(4)
Mn1-N1	1.989(5)	Mn3-O4	2.324(4)
Mn1-O6	1.899(4)	Mn3-O6	1.927(4)
Mn1-O7	2.302(5)	Mn3-N3	1.998(5)
Mn2-O4	2.417(5)	Mn4-O2	1.973(4)
Mn2-O5	1.893(4)	Mn4-O8	2.203(4)
Mn2-O6	1.894(4)	Mn4-O11	1.878(4)
Mn2-O8	1.889(4)	Mn4-O12	1.877(5)
Mn2-O9	2.239(5)	Mn4-N4	2.016(5)
Mn2-N2	2.000(5)	Mn4-N5	2.325(6)
Mn1---Mn2	3.516(9)	Mn2---Mn4	3.671(6)
Mn1---Mn3	2.997(13)	Mn1---Mn4	3.670(6)
Mn2---Mn3	3.228(14)	Mn3---Mn4	3.550(1)

4·ClO_4·DMSO			
Mn1-O7	2.282(6)	Mn3-O1	1.881(5)
Mn1-O10	1.916(5)	Mn3-O2	1.959(5)
Mn1-O11	2.252(5)	Mn3-O3	2.175(5)
Mn1-N1	2.000(6)	Mn3-O4	2.349(6)
Mn1-O6	1.906(5)	Mn3-O6	1.919(5)
Mn1-O3	1.890(5)	Mn3-N3	1.996(6)
Mn2-O4	2.431(6)	Mn4-O12	1.876(6)
Mn2-O5	1.886(6)	Mn4-O8	2.129(5)
Mn2-O6	1.895(5)	Mn4-O11	1.866(5)
Mn2-O8	1.891(5)	Mn4-O13	2.732(9)
Mn2-O9	2.227(6)	Mn4-N4	2.001(6)

Mn2-N2	1.997(6)	Mn4-O2	1.955(5)
Mn1---Mn2	3.532(6)	Mn2---Mn4	3.587(1)
Mn1---Mn3	2.990(16)	Mn1---Mn4	3.654(7)
Mn2---Mn3	3.233(16)	Mn3---Mn4	3.505(1)

Magnetic Properties

Given the structural and chemical similarity in the pairs of trinuclear complexes **1** and **2** and tetranuclear complexes **3** and **4**, we present and discuss the magnetic behavior for complexes **1** and **2** first, followed by the discussion of magnetism for complex **3**.

1·2H$_2$O and 2·H$_2$O·MeOH. These complexes contain the central high-spin Mn^{II} ion (S = 5/2) and two peripheral high-spin Mn^{III} ions (S = 2 each), which provide the expected spin-only value of χT = 10.38 emu mol^{-1} K in the absence of magnetic exchange. Temperature-dependent magnetic susceptibility measurements (Fig. 6) revealed that at 300 K the χT values for both **1**·2H$_2$O and **2**·2H$_2$O·MeOH are lower, 8.46 and 10.36 emu mol^{-1} K, respectively. In both cases, the χT curve exhibits a substantial decrease as the temperature is lowered. These observations are in accord with antiferromagnetic exchange interactions between the central Mn^{II} ion and the peripheral Mn^{III} ions. Fitting the high-temperature part of the inverse susceptibility plot to the Curie-Weiss law afforded the values of the Curie (C) and Weiss (θ) constants, C = 12.32(8) emu mol^{-1} K and θ = –134(2) K for **1**·2H$_2$O and C= 12.75(4) emu mol^{-1} K and θ = –67.0(8) K for **2**·2H$_2$O·MeOH. The Curie constants are similar and significantly higher than the sum of expected spin-only values for uncoupled S = 5/2 and two S = 2 centers. This difference can be explained by the orbital contribution to the total moment of the Mn^{III} ion. The negative Weiss constants are in agreement with the antiferromagnetic exchange coupling in the trimers, although the exchange interaction in **1**·2H$_2$O is much stronger than in **2**·2H$_2$O·MeOH.

The magnetic properties of the trimers were modeled using the Heisenberg-Dirac-Van Vleck Hamiltonian (1),

$$\hat{H} = -2J_1(\hat{S}_1\hat{S}_2 + \hat{S}_2\hat{S}_3) - 2J_2\hat{S}_1\hat{S}_3 + \sum_i \mu_B g_i \hat{S}_i \vec{H}\,, \qquad (1)$$

where S_1, S_2, $S_3$are the spin states and g_1, g_2, g_3 are the g-factors of Mn^{III}, Mn^{II}, and Mn^{III} ions, respectively, J_1 is the exchange coupling constant for the interaction between the central Mn^{II} and peripheral Mn^{III} ions, and J_2 is the weaker interaction between the peripheral Mn^{III} ions. The

mean-field correction (zJ') was also included to account for intermolecular dipolar coupling at lower temperatures. To avoid overparametrization during the fitting procedure, it was reasonably assumed that $g_2 = 2.00$ and $J_2 = 0$ based on the earlier reports of magnetic behavior for similar trinuclear Mn^{III}–Mn^{II}–Mn^{III} clusters.[39-43] In addition, $g_1 = g_3 = g$ due to the symmetry of the clusters **1** and **2**. The best fit to the experimental data was obtained with $J_1 = –7.36(2)$ cm^{-1}, $g = 2.11(1)$, $zJ' = –0.26(1)$ cm^{-1} for **1**·2H_2O ($R^2 = 0.9997$). In the case of **2**·2H_2O·MeOH, however, the three-parameter model could not provide a satisfactory fit to the data, and therefore the g_2 parameter was also allowed to vary, which led to an acceptable fit with $J_1 = –5.04(6)$ cm^{-1}, $g = 2.38(1)$, $g_2 = 1.84(1)$, $zJ' = –0.079(5)$ cm^{-1} ($R^2 = 0.9976$). The refined g_2 value, however, is somewhat low and atypical for the high-spin Mn^{II} ion.

Both **1** and **2** exhibit antiferromagnetic nearest-neighbor exchange interactions that result in the ground state spin of 3/2. The more negative value of the J_1 exchange constant observed for cluster **1** can be explained by the shorter separation between the Mn^{II} and Mn^{III} centers in **1** (3.477 Å) as compared to **2** (3.522 Å). Indeed, an examination of the correlation between J_1 and the $Mn^{II}\cdots Mn^{III}$ separation in these and related carboxylato-supported $Mn^{III}Mn^{II}Mn^{III}$ trimers revealed that this relationship can be described, rather approximately, as $J_1 = A + Bd$ ($Mn^{II}\cdots Mn^{III}$), where $A = –1.3(3)\times10^2$ cm^{-1} and $B = 36(8)$ cm^{-1}/Å (Fig. 7).We note that the $Mn^{II}\cdots Mn^{III}$ separation in **2** is one of the longest observed in such trimers. This observation might explain the imperfection of the presented isotropic model for treatment of magnetism in complex **2** and the somewhat abnormal value of the g_2 parameter.

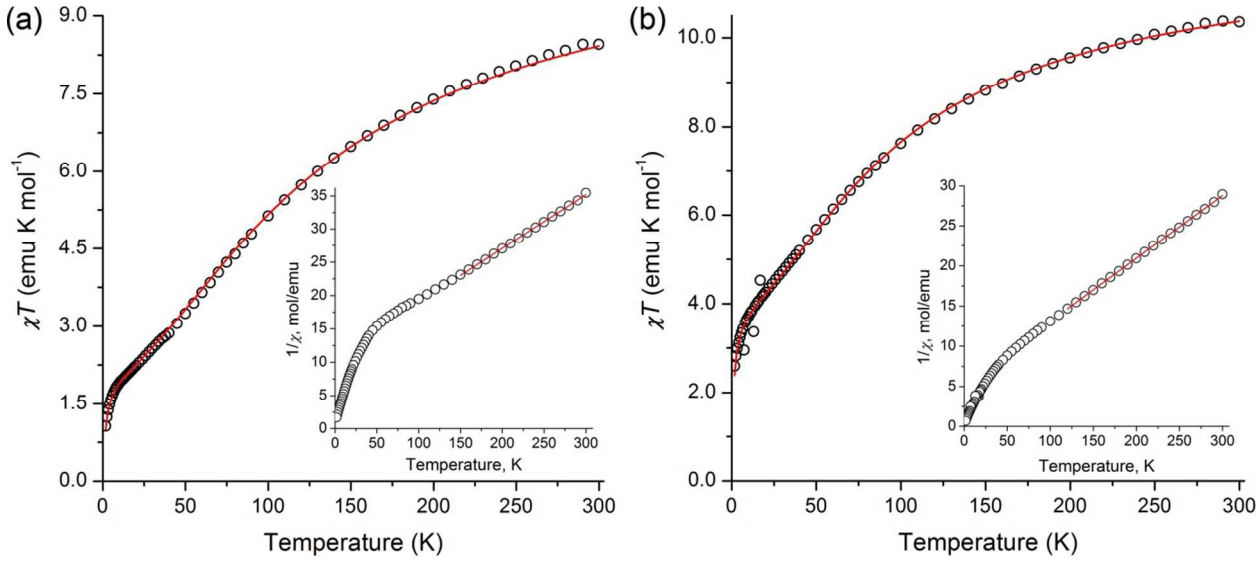

Fig. 6 The temperature dependence of χT for (a) **1**·2H_2O and (b) **2**·2H_2O·MeOH. The solid red lines represent the best fit to the experimental data. The insets show the corresponding temperature dependence of inverse susceptibility and the fit to the Curie-Weiss law in the high-temperature region (solid red lines).

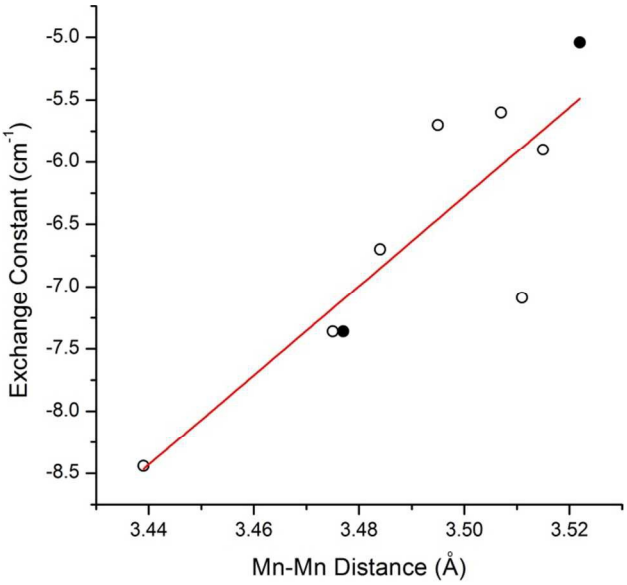

Fig. 7 The magnetic exchange constant (J_1) between the central Mn^{II} and peripheral Mn^{III} ions in the carboxylate-supported Mn^{III}-Mn^{II}-Mn^{III} trimers as a function of the $Mn^{II}\cdots Mn^{III}$ separation. The data established in this work are indicated with filled circles.

3·ClO₄·DMSO.The paramagnetic core in clusters **3** contains four high-spin Mn^{III} ions (S = 2 each) with irregular Mn···Mn separations (Fig. 8a). Similar to clusters **1** and **2**, the temperature dependence of χT for **3** reveals significant antiferromagnetic correlations (Fig. 9), with the room-

temperature value of 11.05 emu mol^{-1} K. Fitting the high-temperature part of the inverse susceptibility plot to the Curie-Weiss law resulted in C = 12.9(3) emu mol^{-1} K and θ = –48(7) K (Fig. 9, inset). The Curie constant (C) is slightly higher than the spin-only expectation value for four uncoupled S = 2 centers (12.0 emu mol^{-1} K). The discrepancy is attributed to the orbital contribution of the Mn^{III} ion. The negative Weiss constant (θ) indicates dominant antiferromagnetic exchange coupling between the Mn^{III} centers, which results in the χT quickly decreasing below 100 K and approaching zero at 1.8 K.

The strength of magnetic coupling in clusters with octahedral high-spin Mn^{III} ions strongly depends on the orientation of the elongated Jahn-Teller axis that defines the magnetic σ-type 3*d* orbital.[44] An examination of the metric parameters in cluster **3** (Table 3) reveals that the Mn2-O4-Mn3 superexchange pathway (J_1)involves the magnetic σ-type orbitals on both Mn^{III} centers, the Mn1−O3−Mn3, Mn1−O11−Mn4, and Mn2−O8−Mn4pathways (J_2) each involve such an orbital on only one of the Mn^{III} centers, and finally, the Mn1−O6−Mn2 and Mn3−O2−Mn4 pathways (J_3) do not involve such orbitals at all (Fig. 8b). Each of the six superexchange pathways, however, involves π-type 3*d* orbitals of the Mn^{III} ions. Based on these symmetry considerations, one could expect antiferromagnetic J_1 and J_3, as they are dominated by interactions between magnetic orbitals of the same symmetry. The J_2 interaction contains both σ-π and π-π contributions, and therefore its absolute value is expected to be smaller but its sign cannot be clearly predicted. Consequently, the magnetic behavior of **3** was modeled using three different exchange parameters with the above-set restrictions (J_1< 0, J_3< 0, $|J_2| << |J_1|$):

$$\hat{H} = -2J_1\hat{S}_2\hat{S}_3 - 2J_2(\hat{S}_1\hat{S}_3 + \hat{S}_1\hat{S}_4 + \hat{S}_2\hat{S}_4) - 2J_3(\hat{S}_1\hat{S}_2 + \hat{S}_3\hat{S}_4) + \sum_i \mu_B g_i \hat{S}_i \vec{H}\,, \qquad (2)$$

where S_i and g_i are the spin state and g-factor of each Mn^{III} ion. To avoid overparametrizaiton, the g_i values were set equal for all four Mn^{III} centers. The best fit to the experimental data was achieved with g = 2.085(6), J_1 = –5.2(1) cm^{-1}, J_2 = 0.098(8) cm^{-1}, and J_3 = –5.4(1) cm^{-1} (R^2 = 0.9989). We note that the low symmetry of cluster **3** suggests the three-*J* model used is certainly an oversimplification. Nevertheless, it provides a good fit to the experimental data and allows a reasonable estimate of the magnetic exchange coupling parameters in this complex.

In spite of our several attempts we are unable to isolate the pure crystals of the complex **4** in bulk form. For that reason we intentionally exclude the magnetic property of complex **4** here.

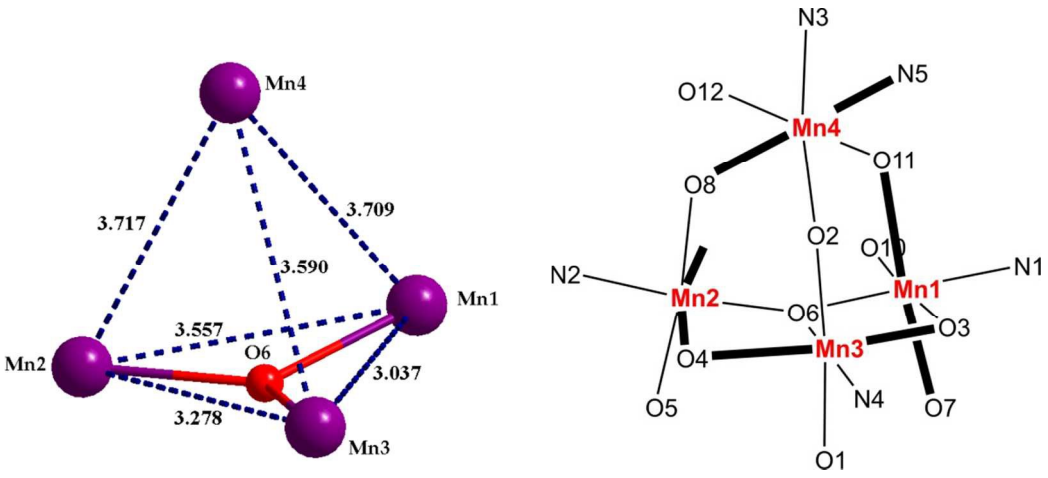

(a) (b)

Fig. 8 (a) Mn···Mn distances within the labeled core of **3**; (b) the nearest environment of octahedrally coordinated Mn^{III} ions, with the elongated Jahn-Teller axes highlighted as bold bonds.

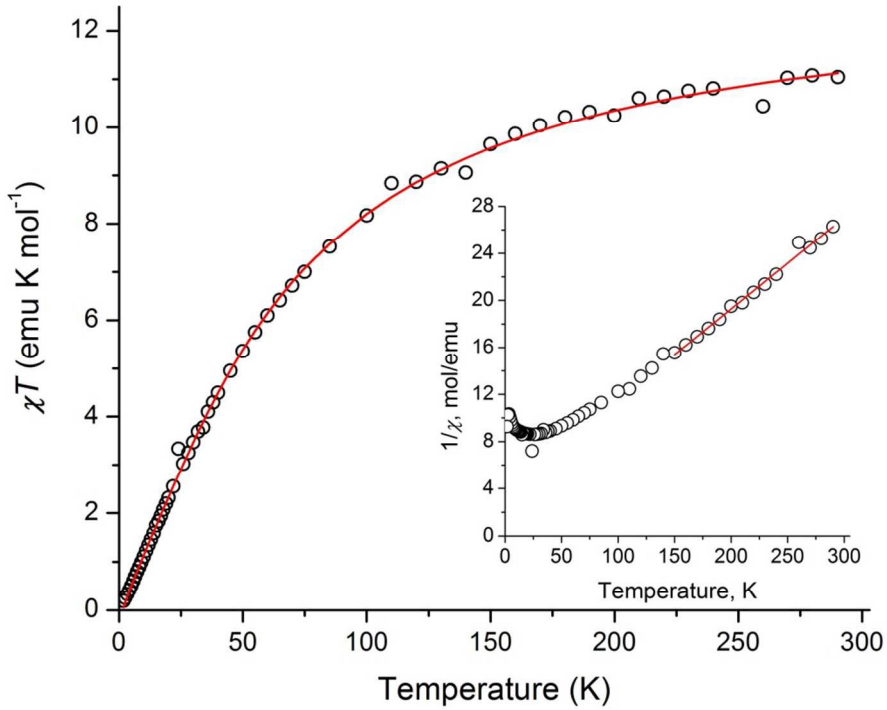

Fig. 9 The temperature dependence of χT for **3**·ClO_4·DMSO. The solid red line represents the best fit to the experimental data. The inset shows the temperature dependence of inverse susceptibility and the fit to the Curie-Weiss law in the high-temperature region (solid red line).

Catechol Oxidation Study

In this work we examined the ability of our [Mn_3] and [Mn_4] assemblies to act as catalysts in the oxidation of 3,5-di-tert-butylcatechol (3,5-DTBC) to the corresponding quinone by UV-vis spectrophotometry. Presence of tertiary butyl groups at 3 and 5 positions on the catechol substrate provides low redox potential for oxidation to 3,5-di-tert-butylquinone (3,5-DTBQ) while preventing further oxidation and ring-opening reaction.[45] The formation of 3,5-DTBQ which exhibits an absorption maximum at ~400 nm can be monitored for this reaction catalyzed by the manganese complexes.

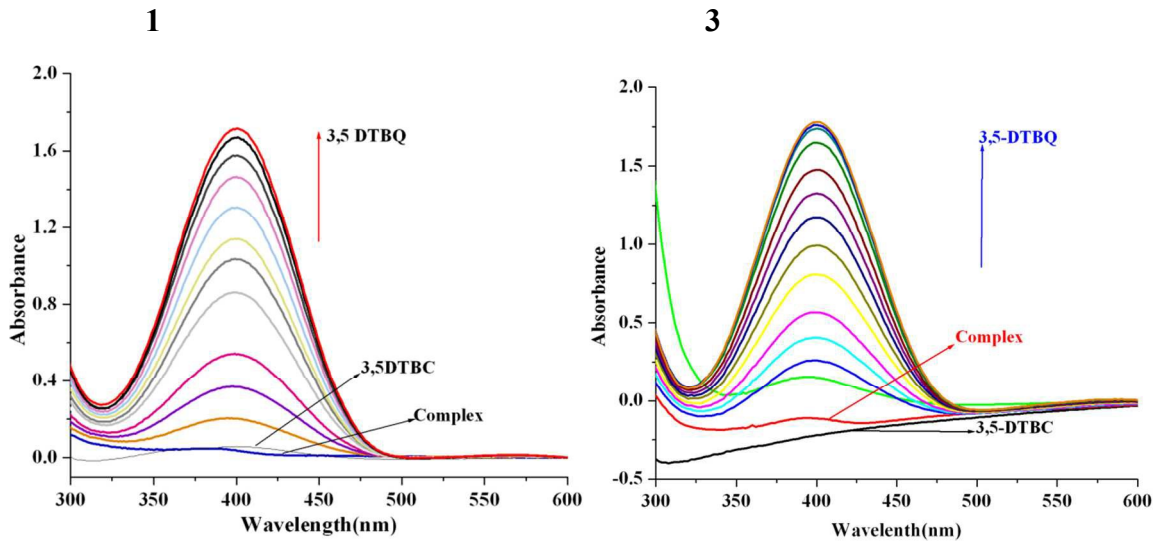

Fig. 10 Increase of absorption spectra after addition of 100 equiv of 3,5-DTBC to a solution containing complexes **1** (left) and **3** (right) (1×10^{-6} M) in MeCN. The spectra were recorded after every 2 min (for **1**) and 5 min (for **3**) up to 1 h.

Complexes **1**–**4** in ~1×10^{-6} M solutions were reacted with a 100-fold concentrated solutions of 3,5-DTBC. The time dependent UV-vis spectra of the mixture were recorded in MeCN and MeOH under aerobic condition up to 1 h. Spectral changes of **1** and **3** in MeCN after addition of 3,5-DTBC are shown in Fig. 10 (Fig. S6 for **2** in the ESI). In both the cases addition of 3,5-DTBC causes a red shift in absorption band of complexes from 382 nm (for **1**) and 390 nm (for **3**) to 400 nm with a gradual increase of absorption intensity. These clearly indicate catalytic oxidation of 3,5-DTBC to 3,5-DTBQ) in solution. However generation of the quinone band was not observed during the course of experiment in pure MeOH, which clearly point out that these complexes were not suitable for oxidation of 3,5-DTBC in MeOH (Fig. S7, ESI).[46] Control experiments in MeCN and air using manganese(II) acetate and manganese(II) perchlorate under

analogous conditions did not show any oxidation of 3,5-DTBC to 3,5-DTBQ. Within 2 h of mixing of the metal salts and substrate in solution the reaction did not demonstrate any amount of 3,5-DTBQ formation.

Kinetic Study for Catechol Oxidation. The kinetic study of the oxidation of 3,5-DTBC to 3,5-DTBQ by the complexes **1-4** were carried out by monitoring the growth of the absorbance at 400 nm by the initial rates method. The experiments were done at a constant temperature of 25 °C and under aerobic condition. For a particular complex–substrate mixture, a time scan at the maximum of the quinone band was carried out for a period of 1 h in MeCN. The rate of oxidation is dependent on the substrate concentration which was examined using 10^{-6} M solutions of **1** and **3** and increasing amounts of 3,5-DTBC (from 10 to 100 equiv). In all cases, first order dependence was observed at low substrate concentrations, whereas saturation kinetics was found at higher substrate concentrations (Fig. 11) (Fig. S8 in the ESI for complexes **2** and **4**). The rate constant for a particular complex/substrate mixture was determined from the log[Aα/(Aα−At)] vs time plot. This type of saturation rate dependence on the concentration of the substrate may be explained by considering the Michaelis−Menten equation for enzymatic kinetics describing the rate of enzymatic reactions by relating the reaction rate to the substrate concentration.[47] A treatment on the basis of Michaelis−Menten approach was consequently applied and linearized by means of Lineweaver−Burk plot (double reciprocal plot) to calculate various kinetic parameters such as Michaelis−Menten constant and the maximum rate (V_{max}) achieved by the system, at maximum (saturating) substrate concentrations.[48] The Michaelis constant K_m is the substrate concentration at which the reaction rate is half of V_{max}, and is an inverse measure of the substrate's affinity for the compound behaving as enzyme.

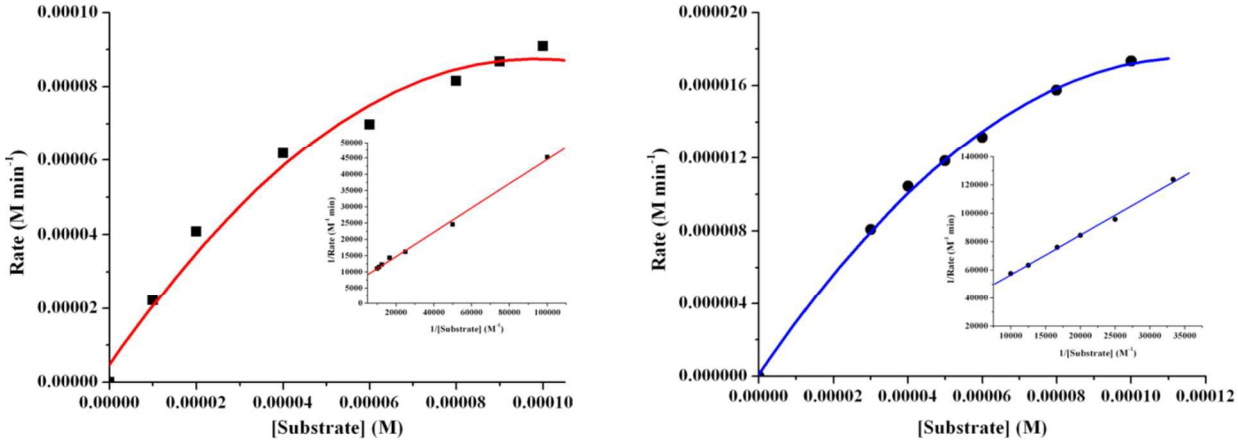

Fig. 11 Plot of initial rates *vs* substrate concentration for the oxidation reaction catalyzed by complexes **1** (left) and **3** (right). Inset shows the Lineweaver−Burk plots.

The turnover number (k_{cat}) values can be calculated by dividing the V_{max} values by the concentration of the corresponding complexes and the kinetic parameters are listed in Table 4. Determination of turnover number (k_{cat}) of the model catalyst is important to understand their relative efficiency. The turnover numbers (k_{cat}) for trinuclear compounds are about four times higher than that of tetranuclear compound. The title compounds are the first examples of trinuclear mixed-valence Mn^{III}/Mn^{II} and tetranuclear Mn^{III} compounds showing catechol oxidase activity. The turnover numbers for these complexes are much higher than those found for other manganese complexes.[49,50]

Table 4. Kinetic parameters for compounds **1-4** obtained at 25°C in MeCN medium.

Compound	V_{max} (M s^{-1})	Std. error	K_m (M)	Std. error	k_{cat} (h^{-1})
1	1.3717 X 10^{-4}	2.21 X 10^{-5}	5.1164 X 10^{-5}	1.01 X 10^{-6}	8.220 X 10^{3}
2	1.5019 X 10^{-4}	1.79 X 10^{-5}	7.4947 X 10^{-5}	1.32 X 10^{-6}	9.011 X 10^{3}
3	3.4730 X 10^{-5}	4.89 X 10^{-5}	9.7106 X 10^{-5}	9.68 X 10^{-6}	2.082 X 10^{3}
4	3.1092 X 10^{-5}	7.02 X 10^{-5}	7.8664 X 10^{-5}	7.12 X 10^{-6}	1.865 X 10^{3}

The mass spectral (ESI-MS positive) characterization of compounds **1**, **3** and 1:100 mixtures with 3,5-DTBC within 10 min of mixing in MeCN were carried out to get an insight into the nature of possible compound-substrate intermediates for catechol oxidation (Fig. S9−S12, ESI). Compound **1** exhibits a base peak at m/z = 194.12, which can be assigned to the protonated ligand $[H_3dmp]^+$ ($C_{11}H_{16}NO_2$). In addition, peaks at m/z = 438.13, 287.06 and 246.03 indicate the

presence of $[Mn^{IV}(dmp)_2H]^+$ ($C_{22}H_{27}MnN_2O_4$), $[Mn^{II}(dmp)(H_2O)Na]^+$ ($C_{11}H_{15}MnNO_3Na$) and $[Mn^{III}(dmp)]^+$ ($C_{11}H_{13}MnNO_2$), respectively. Whereas compound **3** displays a base peak at *m*/*z* = 324.04, which can be assigned to the cationic solvent bound species $[Mn^{III}(dmp)(DMSO)]^+$ ($C_{13}H_{19}MnNO_3S$). A common low intensity peak for both the compounds at *m*/*z* = 683.15 arises due to the dimanganese species $[Mn^{IV}Mn^{III}(dmp)_3]^+$ ($C_{33}H_{39}Mn_2N_3O_6$). The additional peaks in spectrum of **1** are also present in spectrum of **3**, which indeed confirm the higher stability of the catalytically active mononuclear fragments in MeCN. It is interesting to note that the mass spectra of **1** and **3** are almost same after the addition of 3,5-DTBC. In both cases, the spectra exhibit two peaks at *m*/*z* = 243 and 463 which correspond to the quinone–sodium aggregates $[(3,5\text{-DTBQ})Na]^+$ ($C_{14}H_{20}O_2Na$) and $[(3,5\text{-DTBQ})_2Na]^+$ ($C_{28}H_{40}O_4Na$), respectively. There is also another peak at *m*/*z* = 466.18 indicating the presence of the 1:1 mononuclear species–substrate aggregates $[Mn^{III}(dmp)(3,5\text{-DTBQ})]^+$ ($C_{25}H_{33}MnNO_4$). Therefore, the ESI-MS spectra allow us to conclude that the complex−substrate intermediates are formed during oxidation reactions by O_2 of air.

Plausible Mechanistic Considerations of Catechol Oxidation

On the basis of mass spectroscopic evidence, a possible mechanism for the catechol oxidation by compound **A** (*m/z*= 438.13), as depicted in Scheme 1 is proposed. In the first step of the reaction, the catechol coordinates to **A** with removal of one ligand and forms intermediate $[Mn^{IV}(L^2)(3,5\text{-DTBC})]$ (**B**, *m/z*= 466.18). Internal electron transfer within **B** produces a semiquinone bound intermediate $Mn^{III}(L^2)(3,5\text{- DTBSQ})$ (**C**). The species **C** then reacts with dioxygen from air to generate an oxygenated species (**D**) which oxidizes the Mn^{III} center and releases 3,5-DTBQ and hydrogen peroxide. After the quinone molecule is released, the ligand then binds to the metal center to regenerate **A** and the catalytic cycle can continue. Though we could not isolate species **C** and **D** in the solution, we proposed this tentative mechanistic cycle very much similar to those reported in the literature. [51] The availability of ligand bound Mn^{IV} species in solution is higher in case of **1**, which leads to higher turn-over number for the experiment.[31,32] Therefore, it is reasonable to conclude that in the catalytic cycle ligand bound Mn^{IV} fragment can undergo two electron reduction with concomitant oxidation of 3,5-DTBC to 3,5-DTBQ in the presence of molecular oxygen. Indeed, several factors must be considered is assessing the difference in

Scheme 1 Proposed mechanism of catechol oxidation catalyzed by $[Mn^{IV}(dmp^2)_2H]^+$ (**A**)

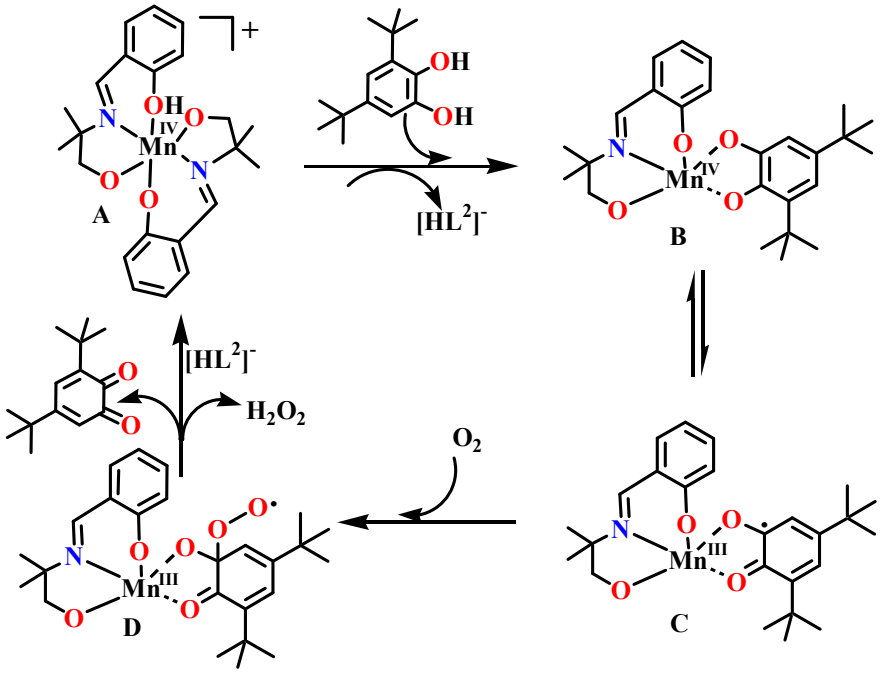

oxidation activities of complexes **1**-**4**, such as substrate association affinity, mode of binding of substrate, electrochemical potential values, ancillary donors and steric match. With respect to the catalytic turnover number (k_{cat}), we may conclude that the reactivity in the oxidation of 3,5-DTBC increases in the order **4** < **3** < **2** < **1**.

Conclusion

In summary, we have demonstrated for the first time the use of same tridentate alcohol-phenol arm bearing ligand, 2-[(2-hydroxy-1,1-dimethyl-ethylimino)-methyl]-phenol for the growth of two trinuclear $Mn^{III}_2Mn^{II}$ and two tetranuclear Mn^{III}_4 complexes **1**-**4**. The work establishes the potential of the ligand in its doubly deprotonated form (both phenol and alcohol end) to enforce the formation of Mn aggregates of varying nuclearity and contrasting molecular topology. In both the deprotonated alcohol ends are essential for the aggregation of Mn ions. The syntheses of the complexes were explored in detail to identify conditions that led to the specific nuclearity, resulting in either a linear carboxlate-supported trinuclear structure or in an adamantane-like tetranuclear structure built around oxido-centered Mn_3 triangle. The magnetic behavior of mixed-

valent linear trimers **1** and **2** is dominated by antiferromagnetic exchange between the central Mn^{II} ion and the peripheral Mn^{III} ions, which leads to the $S = 3/2$ ground state. A comparison to the related trimers found in the literature revealed that the strength of this exchange coupling correlates well with the $Mn^{II}\cdots Mn^{III}$ separation. The magnetic behavior of tetranuclear complex **3** is primarily dependent on the orientation of the elongated Jahn-Teller axes of the four octahedrally coordinated Mn^{III} ions. As a result, the magnetism is dominated by antiferromagnetic exchange in two different pairs of ions, leading to the overall singlet ground state. Kinetic studies in solution revealed that both the trinuclear and tetranuclear complexes are efficient catalysts for the solvent dependent oxidation of 3,5-di-tert-butylcatechol by O_2, with complex **2** being the most active. In MeOH medium all complexes are characteristically inactive. In MeCN the reactivity for the oxidation of 3,5-DTBC increases in the order **4** < **3** < **1** < **2**. The ESI-MS (positive) evidences suggest the presence of metal complex–catechol substrate aggregates with bidentate catechol units to Mn centers.

Acknowledgments

We are very much thankful to the reviewers at the revision stage for their valuable and most appropriate suggestions in improving the standard of the manuscript. MP is thankful to the Council of Scientific and Industrial Research, New Delhi, India for financial support toward her doctoral degree. The authors give thanks to DST, New Delhi, for providing the Single Crystal X-ray Diffractometer facility in the Department of Chemistry, IIT Kharagpur under its FIST program. MP also gives thanks to Dr. Debiranjan Tripathy for fruitful discussion. The work on the molecular magnetism by the FSU group was partially supported by the National Science Foundation (award NSF-0911109).

References

1 G. E. Kostakis, A. M. Ako and A. K. Powell. *Chem. Soc. Rev*., 2010, **39**, 2238−2271.

2 (a) A. M. Mowson, Tu N. Nguyen, A. K. Abboud and G. Christou, *Inorg. Chem*., 2013, **52**, 12320-12322; (b) M. Sarkar, V. Bertolasi and D. Ray, *Eur. J. Inorg. Chem.*, 2010, 2530−2536.

3 (a) M. T. Caudle, J. W. Kamp, M. L. Kirk, P. G. Rasmussen and V. L. Pecoraro, *J. Am. Chem. Soc*., 1997, **119**, 9297−9298; (b) F. Habib, G. Brunet, F. Loiseau, T. Pathmalingam, T. J.

Burchell, A. M. Beauchemin, W. Wernsdorfer, R. Clérac and M. Murugesu, *Inorg. Chem.*, 2013, **52**, 1296–1303.

4 (a) K. N. Ferreira, T. M. Iverson, K. Maghlaoui, J. Barber and S. Iwata, Science, 2004, **303**, 1831−1838; (b) T. G. Carrell, A. M. Tyryshkin and G. C. J. Dismukes, Biol. *Inorg. Chem.*, 2002, **7**, 2−22; (c) R. M. Cinco, A. Rompel, H. Visser, G. Aromí, G. Christou, K. Sauer, M. P. Klein, and V. K. Yachandra, *Inorg. Chem*., 1999, **38**, 5988−5998; (d) V. K. Yachandra, K. Sauer and M. P. Klein, *Chem. Rev*., 1996, **96**, 2927−2950.

5 V. L. Pecoraro, Manganese Redox Enzymes; VCH: New York, 1992.

6 A. Zouni, H. T. Witt, J. Kern, P. Fromme, N. Krauss, W. Saenger and P. Orth, Nature, 2001, **409**, 739−743.

7 N. Kamiya and J. R. Shen, *Proc. Natl. Acad. Sci. U. S. A.*, 2003*,* **100***,* 98-103.

8 (a) K. N. Ferreira, T. M. Iverson, K. Maghlaoui, J. Barber and S. Iwata, *Science*, 2004, **303**, 1831−1838; (b) J. Biesiadka, B. Loll, J. Kern, K.-D. Irrgang, and A. Zouni, *Phys. Chem. Chem. Phys.*, 2004, **6**, 4733−4736.

9 S-Y. Chen, C. C. Beedle, P-R. Gan, G-H. Lee, S. Hill and E-C. Yang, *Inorg. Chem*., 2012, **51**, 4448−4457.

10 A. Saha, K. A. Abboud and G. Christou, *Inorg. Chem*., 2011, **50**, 12774−12784.

11 P-P. Yang, C-Y. Shao, L-L. Zhu and Y. Xu, *Eur. J. Inorg. Chem.*, 2013, 5288−5296.

12 L. Zhang, C. I. Onet, R. Clérac, M. Rouzières, B. Marzec, M. Boese, M. Venkatesan and W. Schmitt, *Chem. Commun*., 2013, **49**, 7400–7402.

13 P. Kar, Y. Ida, T. Kanetomo, M. G. B. Drew, T. Ishida and A. Ghosh, *Dalton Trans*., 2015, **DOI:** 10.1039/C5DT00709G.

14 (a) P. Wang, G. P. A. Yap and C. G. Riordan, *Chem. Commun*., 2014, **50**, 5871–5873; (b) S. K. Dey and A. Mukherjee, *New J. Chem.*, 2014, **38**, 4985—4995; (c) A. Biswas, L. K. Das, M. G. B. Drew, G. Aromí, P. Gamez and A. Ghosh, *Inorg. Chem.*, 2012, **51**, 7993–8001.

15 G. Maayan and G. Christou, *Inorg. Chem*., 2011, **50**, 7015–7021.

16 (a) M. Dey, C. P. Rao, P. K. Saarenketo and K. Rissanen, *Inorg. Chem. Commun*., 2002, **5**, 380–383; (b) M. Dey, C. P. Rao, P. K. Saarenketo, K. Rissanen, E. Kolehmainen and P. Guionneau, *Polyhedron*, 2003, **22**, 3515–3521; (c) M. Dey, C. P. Rao, P. K. Saarenketo, K.

Rissanen and E. Kolehmainen, *Eur. J. Inorg. Chem.*, 2002, 2207−2215; (d) M. Dey, C. P. Rao, P. K. Saarenketo and K. Rissanen, *Inorg. Chem. Commun*., 2002, **5**, 924–928.

17 G. A. Bain, J. F. Berry, *J. Chem. Educ.*, 2008, **85**, 532−535.

18 *Saint, Smart and XPREP;* Siemens Analytical X-ray Instruments Inc.: Madison, WI, 1995.

19 Sheldrick, G. M. SADABS: *Software for Empirical Absorption Correction*; University of Göttingen, Institute fur AnorganischeChemiederUniversitat, Göttingen, Germany, 1999–2003.

20 (a) G. M. Sheldrick, *SHELXS-97,* University of Göttingen, Göttingen,Germany, 1997; (b) G. M. Sheldrick, *SHELXL 97*, *Program for Crystal Structure Refinement*, University of Göttingen, Göttingen, Germany,1997.

21 (a) H. Miyasaka, K. Nakata, L. Lecren, C. Coulon, Y. Nakazawa, T. Fujisaki, K. Sugiura, M. Yamashita and R. Clérac, *J. Am. Chem. Soc*., 2006, 128, 3770–3783; (b) A. Das, K. Gieb, Y. Krupskaya, S. Demeshko, S. Dechert, R. Klingeler, V. Kataev, B. Büchner, P. Müller and F. Meyer, *J. Am. Chem. Soc*., 2011, **133**, 3433−3443; (c) M. Hirotsu, Y. Shimizu, N. Kuwamura, R. Tanaka, I. Kinoshita, R. Takada, Y. Teki and H. Hashimoto, *Inorg. Chem*., 2012, **51**, 766−768.

22 G. B. Deacon and R.J. Phillips, *Coord. Chem. Rev*., 1980, **33**, 227–250.

23 S. Demeshko, G. Leibeling, W. Maringgele, F. Meyer, C. Mennerich, H. H. Klauss and H. Pritzkow, *Inorg. Chem.*, 2005, **44**, 519–528.

24 F. Arjomandirad, J. Talat-Mehrabad, N. Ziaifar and B. Shaabani, *Arch. Appl. Sci. Res.*, 2011, **3**, 480–484.

25 Nakamoto, K. *Infrared and Raman Spectra of Inorganic and Coordination Compounds*, 4th ed.; Wiley: New York, 1986.

26 R. Thomas, C. B. Shoemaker and K. Eriks, *Acta Crystallogr.*, 1966, **21**, 12–20.

27 F. A. Cotton, E. V. Dikarev, M. A. Petrukhina and S.-E. Stiriba, *Inorg. Chem.*, 2000, **39**, 1748–1754.

28 E. Krickemeyer, Y. Kaiser, A. Stammler, H. Bögge and T. *Z.* Glaser, *Anorg. Allg. Chem*., 2013, 1527–1533

29 R. Cini, *Acta Crystallogr*., *Sect. C*, 2001, **57**, 1171–1173.

30 H. H. Thorp, *Inorg. Chem*., 1992, **31***,* 1585–1588.

31 C. Hureau, E. Anxolabéhère-Mallart, G. Blondin, E. Rivière and M. Nierlich, *Eur. J. Inorg. Chem*., 2005, 4808–4817.

32 A. Prescimone, J. Wolowska, G. Rajaraman, S. Parsons, W. Wernsdorfer, M. Murugesu, G. Christou, S. Piligkos, E. J. L. McInnes and E. K. Brechin, *Dalton Trans*., 2007, 5282−5289.

33 A. Yoshino, T. Miyagi, E. Asato, M. Mikuriya, Y. Sakata, K. Sugiura, K. Iwasaki and S. Hino, *Chem. Commun*., 2000, 1475−1477.

34 T. C. Higgs, K. Spartalian, C. J. O'Connor, B. F. Matzanke and C. J. Carrano, *Inorg. Chem*., 1998, **37**, 2263−2272.

35 C. Mukherjee, T. Weyhermüller, K. Wieghardt and P. Chaudhuri, *Dalton Trans*., 2006, 2169−2171.

36 S. Bhaduri, M. Pink and G. Christou, *Chem. Commun*., 2002, 2352–2354.

37 (a) P. Kar, R. Haldar, C. J. Gómez-García and A. Ghosh, *Inorg. Chem*., 2012, **51**; 4265−4273; (b) S. Mukherjee, K. A. Abboud, W. Wernsdorfern and G. Christou, *Inorg. Chem*., 2013, **52**, 873−884.

38 M. Oh, G. B. Carpenter and D. A. Sweigart, *Chem. Commun*., 2002, 2168–2169.

39 (a) Carlin, R. L. *Magnetochemistry*. Springer-Verlag: Berlin, Germany, 1986; (b)D. P. Kessissoglou, M. L. Kirk, M. S. Lah, X. Li, C. Raptopoulou, W. E. Hatfield and V. L. Pecoraro, *Inorg. Chem*., 1992, **31**, 5424−5432.

40 V. Tangoulis, D. A. Malamatari, K. Soulti, V. Stergiou, C. Raptopoulou, A. Terzis, T. A. Kabanos and D. P. Kessissoglou, *Inorg. Chem*., 1996, **35**, 4974−4983.

41 V. Tangoulis, D. A. Malamatari, G. A. Spyroulia, C. Raptopoulou, A. Terzis and D. P. Kessissoglou, *Inorg. Chem*., 2000, **39**, 2621−2630.

42 Y. G. Li, L. Lecren, W. Wernsdorfer and R. Clérac, *Inorg. Chem. Commun*., 2004, **7**, 1281−1284.

43 H. C. Yao, M. M. Li, L. M. Zheng and Z. J. Li, *J. Coord. Chem*., 2008, **61**, 2814−2822.

44 S. G. Baca, I. L. Malaestean, T. D. Keene, H. Adams, M. D. Ward, J. Hauser, A. Neels and S. Decurtins, *Inorg. Chem*., 2008, **47**, 11108−11119.

45 J. Mukherjee, and R. Mukherjee, *Inorg. Chim. Acta*, 2002, **337**, 429−438.

46 (a) T. Chattopadhyay, M. Mukherjee, A. Mondal, P. Maiti, A. Banerjee, K. S. Banu, S. Bhattacharya, B. Roy, D. J. Chattopadhyay, T. K. Mondal, M. Nethaji, E. Zangrando and D. Das, *Inorg. Chem*., 2010, **49**, 3121–3129; (b) K. S. Banu, T. Chattopadhyay, A. Banerjee, S. Bhattacharya, E. Suresh, M. Nethaji, E. Zangrando and D. Das, *Inorg. Chem*., 2008, **47**, 7083−7093.

47 K. S. Banu, T. Chattopadhyay, A. Banerjee, M. Mukherjee, S. Bhattacharya, G. K. Patra, E. Zangrando and D. Das, *Dalton Trans*., 2009, 8755–8764.

48 Wilkins, R. G. *Kinetics and Mechanism of Reactions of Transition Metal Complexes;* Wiley-VCH Verlag GmbH & Co. KGaA: Weinheim, Germany, 2002; p 4.

49 (a) A. Jana, N. Aliaga-Alcalde, E. Ruiz and S. Mohanta, *Inorg. Chem*., 2013, **52**, 7732−7746; (b) V. Gómez and M. Corbella, *Eur. J. Inorg. Chem.*, 2012, 3147–3155; (c) T. J. Hubin, J. M. McCormick, N. W. Alcock and D. H. Busch, *Inorg. Chem.*, 2001, **40**, 435−444; (d) M. U. Triller, D. Pursche, W-Y. Hsieh, V. L. Pecoraro, A. Rompel and B. Krebs, *Inorg. Chem.*, 2003, **42**, 6274−6283.

50 (a) I. A. Koval, P. Gamez, C. Belle, K. Selmeczi and J. Reedijk, *Chem. Soc. Rev*., 2006, **35**, 814−840; (b) V. K. Bhardwaj, N. Aliaga-Alcalde, M. Corbella, and G. Hundal, *Inorg. Chim. Acta*, 2010, **363**, 97−106.

51 (a) Y. Hitomi, A. Ando, H. Matsui, T. Ito, T. Tanaka, S. Ogo and T. Funabiki, *Inorg. Chem*., 2005, **44**, 3473−3478. (b) J. A. R. Hartman, B. M. Foxman and S. R. Cooper, *J. Chem. Soc., Chem. Commun*., 1982, 583−584; (c) A. Caneschi and A. Dei, *Angew. Chem., Int. Ed*., 1998, **37**, 3005−3007.